Modeling Aspects Concerning THUNDER Actuators *

M. Capozzoli[1], J. Gopalakrishnan[2], K. Hogan[3], J. Massad[4], T. Tokarchik[5], S. Wilmarth[6]
and
H.T. Banks[7], K.M. Mossi[8], R.C. Smith[9, †]

[1]Department of Mathematics, University of New Hampshire, Dover, NH 03820
[2,6]Department of Mathematics, Texas A&M, College Station, TX 77843
[3]Department of Mathematics, University of Texas, Austin, TX 78723
[5]Department of Mathematics, University of Tulsa, Tulsa, OK 74105
[4,7,9]Center for Research in Scientific Computation, North Carolina State Univ., Raleigh, NC 27695
[8]FACE International Corporation, Norfolk, VA 23508

Abstract

This paper summarizes techniques for modeling geometric properties of THUNDER actuators which arise in the fabrication process. These actuators are high performance composites comprised of layers of piezoceramics in combination with aluminum, stainless steel, brass or titanium bonded with hot-melt adhesive. During the construction process, the assembly is heated under pressure to high temperatures, cooled and repoled to restore the actuator capabilities. This process provides the actuators with the robustness necessary to withstand the high voltages required for large displacement and force outputs. The process also provides the actuators with their characteristic curved shape. In this paper, relations between the thermal and electrostatic properties of the material and the final geometric configuration are quantified. This provides an initial model that can be employed in control applications which employ THUNDER actuators.

Keywords: THUNDER actuators, piezoceramic materials

1. Introduction

In this paper, we address the modeling of certain static properties of THUNDER actuators which result from the fabrication process. These actuators are typically constructed from layers of piezoceramic wafers, aluminum, stainless steel, brass or aluminum bonded with hot-melt adhesive. To construct the actuators, the assembly is heated under pressure to high temperature and then cooled to room temperature. During cooling, the adhesive solidifies and subsequent cooling leads to the production of internal stresses due to differing thermal properties of the component materials. This yields the characteristic curvature of the material. Once the material is cooled, it must be repoled since the temperatures required for bonding are in the proximity of the Curie temperature. The rotation of dipole moments in the piezoceramic provides a second source of internal stress which reduces the final curvature. This fabrication process significantly enhances the robustness of the actuator with respect to mechanical impacts and voltage levels. As a result of this construction, high voltages can be applied to the actuators and large displacements sustained without causing damage. This provides the actuators with significant strain and force capabilities.

This paper addresses the modeling of actuator properties as motivated by the following two questions. (i) Given a specified material composition and set of manufacturing conditions, what will be the final actuator shape? (ii) What material composition and conditions are required to attain a given actuator configuration? We focus primarily

*This problem was investigated by the first six authors under the direction of the last three authors during the Industrial Mathematics Modeling Workshop for Graduate Students held at North Carolina State University on July 27-August 4, 1998.

†Corresponding author: rsmith@eos.ncsu.edu, (919) 515-7552

on the forward problem (i) which is a necessary first step before addressing the inverse problem (ii). Specifically, we consider the development of a model which quantifies the effects of differing thermal properties and repoling on the final actuator shape.

The quantification of strains due to thermal gradients has been investigated for a variety of applications (e.g., see [1, 2, 3, 4]) with certain aspects having been considered for THUNDER actuators [5]. We extend this analysis to obtain relations specifying the strains at the actuator surface and curvature for THUNDER actuators in terms of thermal properties of the components. The quantification of stresses and strains due to poling is based on domain theory for general ferroelectric materials [6, 7] with certain analogies drawn from ferromagnetic domain theory [8, 9]. The thermal and electrostatic stress are then combined with elasticity theory to provide a model for the induced curvature. While not detailed here, this model can then be employed to specify parameter dependent states in the inverse problem (ii).

Certain details describing the manufacturing process for THUNDER actuators are provided in Section 2 to indicate the conditions under consideration. The thermal model is outlined in Section 3 while the modeling of strains due to repoling is considered in Section 4. In Section 5, the validity of the model, as well as certain limitations, is illustrated through a comparison with experimental data.

2. Manufacturing Process

As depicted in Figure 1, a typical THUNDER actuator is comprised of a piezoceramic wafer, a metallic backing material, hot-melt adhesive layers, and optional metallic top layers. Some standard materials that are used for backing include aluminum, stainless steel, titanium and brass. The adhesive employed by Face International Corporation is the high performance thermoplastic LaRC-SI [10]. The design and performance of the actuator can be modified by varying the number of layers and/or raw materials.

The assemblage is then bonded under the following conditions. The assembled THUNDER components are placed in a vacuum bag (100 kPa) and then heated in an autoclave from room temperature to 204^o C at a rate of 5.6^o C/min. The chamber is then pressurized with nitrogen to 241.3 kPa and the temperature is raised to 325^o C. The composite is maintained under these conditions for 30 minutes and then cooled at a rate of 5.6^o C/min to 52^o C. At this point, both the autoclave pressure and vacuum are released at a gradual rate to minimize mechanical stresses which might crack or break the material. Details concerning the construction process can be found in [11].

The LaRC-SI adhesive solidifies at approximately 270^o C and subsequent bending occurs as the composite is cooled due to differing thermal coefficients of the components. The modeling of the thermal effects on the final curvature is thus considered for temperatures from 270^o C to 25^o C.

The Curie temperature for the employed piezoceramic compound PZT-5A is approximately 350^o C so the previously poled material suffers some loss of polarization in the manufacture process. Hence it must be repoled after cooling through the application of a sustained DC voltage.

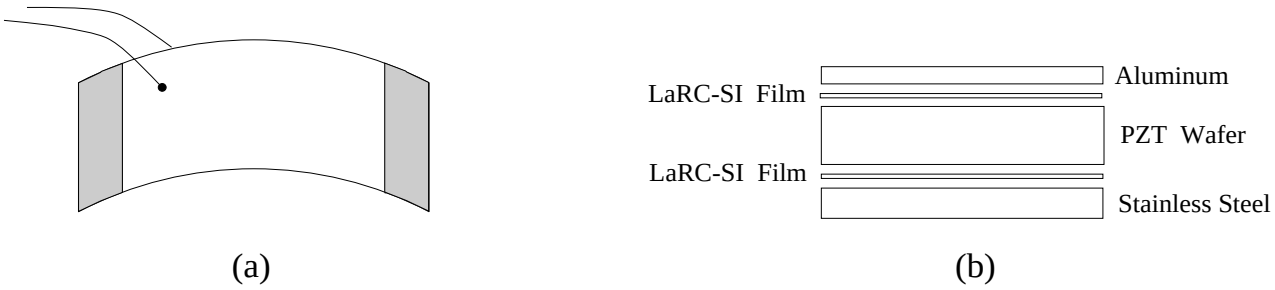

Figure 1. (a) Schematic of a THUNDER actuator; (b) Layers employed in the construction of the composite.

3. Thermal Strains

The primary mechanism which produces the curvature in the cooled actuator is the differing thermal coefficients in the metallic backing and top layers, piezoceramic wafer, and adhesive layers. This produces differential contraction rates as the composite is cooled and yields the subsequent curvature.

To model the thermal strains and corresponding stresses, we assume that the composite is comprised of N layers with the modulus of elasticity and coefficients of thermal expansion for each layer respectively denoted by E_j and α_j. The coordinate system is oriented so that the backing material lies in the x, z-plane with $y = 0$ corresponding to the outer edge of the composite as depicted in Figure 2. The width of the j^{th} layer is denoted by b_j while h_j indicates the y-coordinate of the top edge of the j^{th} layer. Finally, the strain at the $y = 0$ position and curvature at the neutral axis are respectively denoted by ε_0 and k.

The model is derived under the assumptions that linear elasticity and thermal relations can be employed in each layer and that the heating process is uniform. Furthermore, it is assumed that strains in the y and z-directions are negligible. We note that this latter assumption must be revaluated when considering the strains due to poling or actuation due to the magnitude of piezoelectric effect.

Under these assumptions, the total strain $\varepsilon(y)$ at a height y in the composite can be expressed as

$$\varepsilon(y) = \frac{\sigma(y)}{E(y)} + \alpha(y)\Delta t \tag{1}$$

where $\sigma(y)$ denotes the stress and Δt is the change in temperature. The Youngs' modulus and thermal coefficient $E(y)$ and $\alpha(y)$ are the piecewise constant functions given by $E(y) = E_j$ and $\alpha(y) = \alpha_j$ when y is in the j^{th} layer. Furthermore, the assumption that strains are linear in the transverse direction yields the relation

$$\varepsilon(y) = \varepsilon_0 - ky \tag{2}$$

between the strain ε_0 at the outside edge of the composite and the strain at a height y. Combination of (1) and (2) then yields the stress expression

$$\sigma(y) = [\varepsilon_0 - ky - \alpha(y)\Delta T]E(y)\,. \tag{3}$$

Force and moment balancing provides the constraints necessary to solve for ε_0 and k. For a layer having cross sectional area A_j, the forces due to elastic and thermal stresses are

$$F_j = \int_{A_j} \sigma \, dA$$

while the moments are

$$M_j = \int_{A_j} y\sigma \, dA\,.$$

Force balancing provides the relation

$$\begin{aligned} 0 &= \sum_{j=1}^{N} \int_{A_j} \sigma \, dA \\ &= \sum_{j=1}^{N} E_j b_j \left[(h_j - h_{j-1})(\varepsilon_0 - \alpha_j \Delta T) - \frac{1}{2} k (h_j^2 - h_{j-1}^2) \right] \end{aligned}$$

while moment balancing yields

$$\begin{aligned} 0 &= \sum_{j=1}^{N} \int_{A_j} y\sigma \, dA \\ &= \sum_{j=1}^{N} E_j b_j \left[\frac{1}{2} (h_j^2 - h_{j-1}^2)(\varepsilon_0 - \alpha_j \Delta T) - \frac{1}{3} k (h_j^3 - h_{j-1}^3) \right]. \end{aligned}$$

To facilitate the solution of the strain ε_0 and curvature k, we reformulate the constraints as the linear system

$$A\mathcal{E} = f \tag{4}$$

where $\mathcal{E} = [\varepsilon_0, k]^T$ and

$$A = \begin{bmatrix} \sum_{j=1}^{N} E_j b_j (h_j - h_{j-1}) & -\frac{1}{2}\sum_{j=1}^{N} E_j b_j (h_j^2 - h_{j-1}^2) \\ \frac{1}{2}\sum_{j=1}^{N} E_j b_j (h_j^2 - h_{j-1}^2) & -\frac{1}{3}\sum_{j=1}^{N} E_j b_j (h_j^3 - h_{j-1}^3) \end{bmatrix} \tag{5}$$

and

$$f = \begin{bmatrix} \sum_{j=1}^{N} E_j b_j \alpha_j \Delta T (h_j - h_{j-1}) \\ \frac{1}{2}\sum_{j=1}^{N} E_j b_j \alpha_j \Delta T (h_j^2 - h_{j-1}^2) \end{bmatrix}. \tag{6}$$

It is noted that the matrix A and vector f are easily constructed once the geometrical and material properties of the layers in the composite have been specified. Once $\mathcal{E}$ has been determined, the strains at a height y in the material are specified by (2) and the radius of curvature is given by $R = 1/k$. In the next section, we include the strains due to repoling. In combination, this forms the basis for solving the forward problem (i) to determine the effect of manufacturing conditions on the final geometry of the actuator.

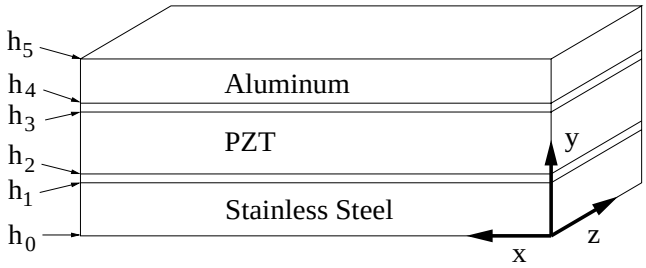

Figure 2. Orientation of the composite THUNDER actuator with five layers.

4. Strains Due to Repoling

Because the THUNDER materials are heated to temperatures in the proximity of the Curie temperature during the manufacturing process, it is necessary to repole the piezoceramic wafer before the composite can be employed as an actuator. This entails the application of large DC voltages to realign dipole moments in the transverse (d_{33}) direction. This causes the piezoceramic wafer to contract longitudinally which produces a subsequent reduction in curvature.

To model the strains generated by the alignment of dipoles in the y-direction, it is necessary to consider certain aspects of ferroelectric domain theory. Details regarding this theory can be found in [6, 7] with analogous theory for ferromagnetic materials provided in [8, 9].

The piezoceramic wafers are in a poled state before the heating process with dipoles aligned in the transverse direction. In general, when these materials are heated above the Curie temperature, the domain structure is lost and the properties of become paraelectric. In this state, the material acts as a normal dielectric. When the temperature is reduced below the Curie temperature, the domain structure reforms to minimize intergranular stresses. The material exhibits no net polarization, however, since the orientation of domains is random. Finally, repolarization through the application of a large applied DC voltage aligns the domains and yields a configuration which provides the material material with its actuator and sensor capabilities. The three stages are depicted in Figure 3. From this figure, it is observed that poling in the transverse direction produces positive strains in the y-direction and corresponding negative strains in the x-direction.

To quantify the spontaneous strain e_y in the material due to dipole ordering, we follow the approach in [8, pages 343-345] or [9, pages 99-104] where analogous relations are developed for ferromagnetic materials. It is first noted that if ϕ is the angle between dipoles in a domain and the y-axis, then the strain varies as

$$e(\phi) = e_y \cos^2 \phi \, .$$

Under the assumption of a random orientation of domains, the strain due to the onset of domain formation is given by

$$\begin{aligned} \lambda_0 &= \int_{-\pi/2}^{\pi/2} e_y \cos^2\phi \sin\phi \; d\phi \\ &= \frac{e_y}{3} \, . \end{aligned}$$

Finally, it follows that the saturation electrostriction λ_s due to dipole alignment during repoling is $\lambda_s = e_y - \lambda_0$ so that

$$\lambda_s = \frac{2}{3} e_y \, . \tag{7}$$

The relation (7) can be utilized in the following manner. The saturation electrostriction λ_s can either be measured or estimated through a least squares fit to data for a given material. The spontaneous transverse strain e_y due to domain alignment is then specified by (7). To determine the effect of polarization on curvature, it is necessary to quantify the resulting strain in the x-direction. This can be accomplished through either a trigonometric analysis similar to that used to obtain (7) or by employing the relation

$$e_x = -\nu e_y$$

where ν denotes the Poisson ratio for the material. The longitudinal strains produced during repoling can then be expressed as

$$e_x = -\frac{3}{2} \nu \lambda_s \tag{8}$$

where ν and λ_s are parameters which must be measured or estimated through a least squares fit to data for a given piezoceramic material.

In the piezoceramic layer, the relation (8) can be combined with the thermal relation (1) to yield

$$\varepsilon(y) = \frac{\sigma(y)}{E(y)} + \alpha(y)\Delta t - \frac{3}{2}\nu\lambda_s \, .$$

For the composite structure, this yields the stress relation

$$\sigma(y) = \left[\varepsilon_0 - ky - \alpha(y)\Delta T + \frac{3}{2}\delta\nu\lambda_s \right] E(y)$$

where

$$\delta = \begin{cases} 1 \, , & \text{if } y \text{ is in the piezoceramic layer} \\ 0 \, , & \text{otherwise} \end{cases}$$

isolates the electrostatic strains due to repoling to the piezoceramic layer. Force and moment balancing in this case yields the A matrix defined in (5) and the modified f vector

$$f = \begin{bmatrix} \sum_{j=1}^{N} E_j b_j (\alpha_j \Delta T - 3/2 \delta\nu\lambda_s)(h_j - h_{j-1}) \\ \\ \frac{1}{2}\sum_{j=1}^{N} E_j b_j (\alpha_j \Delta T - 3/2 \delta\nu\lambda_s)(h_j^2 - h_{j-1}^2) \end{bmatrix} \tag{9}$$

which incorporates the effects of repoling on the stresses in the piezoelectric layer. Solution of the system (4) then provides the strain ε_0 and curvature k which incorporate both thermal and electrostatic effects. The validity and limitations of the model are illustrated in the next section where the characterization of a THUNDER actuator through comparison with data is considered.

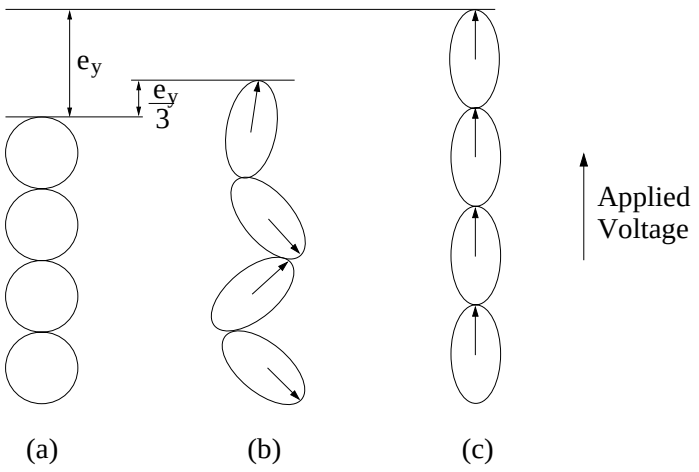

Figure 3. Material behavior of the PZT wafer as it is cooled through the Curie temperature (after Jiles [9]). (a) Material in the paraelectric regime above the Curie temperature; (b) Random domain structure below the Curie temperature; (c) Saturation polarization due to an applied voltage.

5. Model Validation

To illustrate the validity of the model and ascertain possible limitations, we compare the geometries determined by the model with data from a variety of THUNDER actuators designed and constructed by Face International Corporation. The first step necessary for comparison with experimental data is the formulation of the geometry specified by the model with that measured for the actuators. The actuators are constructed with the bottom layer extending beyond the PZT and top layers as illustrated in Figure 1a. The curvature in the region covered by the actuator layer is assumed uniform while the tabs on either side remain unbent since they are not subjected to either thermal or piezoelectric strains. This produces the configuration depicted in Figure 4. The model yields the radius of curvature $R = 1/k$ for the actuator region while the height h', which includes the tabs, is measured for the physical actuators. Furthermore, the actuator length s and length t of each tab are measured for a given actuator. It is thus necessary to quantify the relation between the radius of curvature R, the measured dome height h' and the lengths s and t.

Given the radius of curvature R specified by the model and the measured length s, the subsumed angle θ is given by

$$\theta = \frac{s}{2R}\,.$$

Furthermore, the length t and height h of the tabs are related by the expressions

$$h = t\sin\theta$$

and

$$r + h = R\cos\theta\,.$$

Since $R = r + h'$, it follows directly that

$$h' = R(1 - \cos(s/2R)) + t\sin(s/2R)\,. \tag{10}$$

Given the measured values of s and t, and the radius R specified by the model, the relation (10) provides the dome height h' which can be directly compared with measurements for various actuator configuration.

Four actuators were considered with the dimensions and component materials summarized in Table 1. It is noted that the actuators differ in the metals employed for the bottom layer, the number of layers, and the thicknesses of the individual layers. The values for the modulus of elasticity E and thermal coefficients α reported by manufacturers for the component materials are compiled in Table 2.

The first actuator had a bottom layer constructed from stainless steel and a thin aluminum top layer. The measured values for h', which are reported in Table 3, indicate a 13.6% reduction in the dome height after repoling.

This is in accordance with the explanation in Section 4 that the curvature is reduced when dipole moments align with the applied field in the y-direction. The performance of the model is indicated in Table 3 for two sets of parameters. For the actuator before repoling, the parameters specified by the manufacturers (Parameter Set 1) yields a dome height h' which differs from the measured value by approximately 12%. In the second case, values of E and α were estimated through a least squares fit to the data to obtain the Parameter Set 2 which is summarized in columns 3 and 5 of Table 2. Due to the manner through which these parameters were determined, the corresponding dome height matches the experimental value for the actuator before poling. We note that the estimation of parameters for applications of this type is typically necessary to accommodate the bulk nature of certain mechanisms, introduced during the construction process, and the inherent uncertainties in reported values.

To quantify the strains due to domain rotation during repoling, the Poisson ratio was taken to be $\nu = .3$ and the saturation electrostriction value λ_s = 1.11e-3 was determined to quantify the height after poling. The feasibility of this value is indicated by comparing it with the strain ε_0 = -4.7e-3 computed at the bottom edge of the actuator.

Actuator 2 differs both in the employed materials and the dimensions. It was constructed with a thin brass bottom layer and no top layer. As with Actuator 1, the use of the parameters specified by manufacturers yields a height h' which differs from the measured value by about 16% whereas the estimation of E and α for brass yields parameters which are within 6% of reported values and an exact fit to the height. The parameter values for the remaining layers in this second case were taken to be those estimated for the materials in Actuator 1.

The value of $h' = .388$ cm predicted by the model after repoling is obtained with the saturation electrostriction λ_s = 1.11e-3 estimated for Actuator 1. The accuracy of the prediction attests to the validity of the model used to quantify strains due to domain rotation. Finally, we note that the physical height $h' = .380$ cm can be matched by the model with the parameter λ_s = 1.245e-3.

The third actuator differed from the second in that it had a titanium base layer as compared with the slightly thinner brass layer employed in Actuator 2. Because the thermal coefficient for titanium is significantly smaller than that of brass, the measured dome height is less than half that of Actuator 2. In this case, it is noted that the use of the manufacturer specified parameters (Parameter Set 1) yields a modeled dome height that is within 2.5% of the measured value. Moreover, when the previously estimated parameters for the LaRC-SI and PZT were employed with estimated parameters for titanium, the predicted dome height matches the measured value. Finally, when the saturation electrostriction λ_s = 1.11e-3, determined for Actuator 1, is employed for modeling the piezoelectric strains, the predicted height h' after repoling is within 8.5% of the measured value. This further indicates the accuracy of the domain rotation model used to quantify strains due to repoling.

To test the robustness of the model with parameters estimated for Actuator 1 when the dimensions are changed, the dome height h' of Actuator 4 was measured and compared to the modeled value obtained with Parameter Set 2. It is noted in Table 2 that Actuator 4 is constructed from the same material as Actuator 1 but with significantly different dimensions and layer thicknesses. The measured dome height for Actuator 4 was found to be .339 cm. The modeled height obtained with Parameter Set 1 (manufacturer specifications) was .248 cm while the height predicted with Parameter Set 2 (estimated for Actuator 1) was .304 cm. Hence it is observed that the model with parameters identified for a significantly different configuration predicts the dome height to within 11% accuracy. It is hypothesized that the discrepancy is due to variations introduced in the manufacturing process.

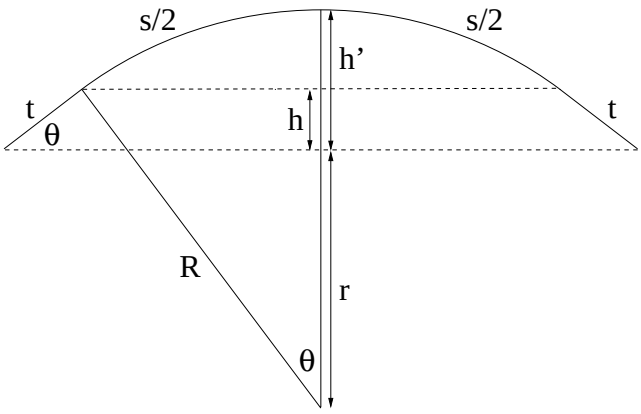

Figure 4. Geometry of the actuator with tabs.

		Materials	Thickness (cm)	Length, Width and Tabs (cm)
Actuator 1	Layer 1	Stainless Steel 304	2.540e-2	
	Layer 2	LaRC-SI	2.540e-3	Length s = 5.08e-3
	Layer 3	PZT-3195Hd	3.810e-2	Width b = 5.08e-3
	Layer 4	LaRC-SI	2.540e-3	Tabs t = 1.27e-3
	Layer 5	Aluminum 3003	2.540e-3	
Actuator 2	Layer 1	Brass	7.620e-3	Length s = 3.81e-3
	Layer 2	LaRC-SI	2.540e-3	Width b = 1.27e-3
	Layer 3	PZT-3195Hd	2.032e-2	Tabs t = 6.35e-4
	Layer 4	LaRC-SI	2.540e-3	
Actuator 3	Layer 1	Titanium	1.016e-2	Length s = 3.81e-3
	Layer 2	LaRC-SI	2.540e-3	Width b = 1.27e-3
	Layer 3	PZT-3195Hd	2.032e-2	Tabs t = 6.35e-4
	Layer 4	LaRC-SI	2.540e-3	
Actuator 4	Layer 1	Stainless Steel 304	7.620e-3	
	Layer 2	LaRC-SI	2.540e-3	Length s = 3.81e-3
	Layer 3	PZT-3195Hd	2.032e-2	Width b = 1.27e-3
	Layer 4	LaRC-SI	2.540e-3	Tabs t = 6.35e-4
	Layer 5	Aluminum 3003	2.540e-3	

Table 1. Components and dimensions of THUNDER actuators.

Materials	Thermal Coefficient α ($10^{-6}/^o$C)		Modulus of Elasticity E (GPa)	
	Manufacturer Specs. (Parameter Set 1)	Estimated Param. (Parameter Set 2)	Manufacturer Specs. (Parameter Set 1)	Estimated Param. (Parameter Set 2)
Aluminum 3003	24.00	22.00	68.95	64.0
Stainless Steel 304	17.30	19.30	193.10	186.0
Brass	20.0	18.72	100.0	95.0
Titanium	9.5	10.67	114.0	114.0
PZT 3195HD	3.0	3.5	67.0	62.0
LaRC-SI	46 (23-150^{o}C)	59.0	3.45	5.0
	60 (150-200^{o}C)	67.0		

Table 2. Values of the thermal coefficients and moduli of elasticity reported by manufacturers and estimated through a fit to data.

	Actuator 1		Actuator 2		Actuator 3	
	Before Poling	After Poling	Before Poling	After Poling	Before Poling	After Poling
Measured h' (cm)	.445	.385	.452	.380	.194	.141
Modeled h' (cm) (Parameter Set 1)	.392		.525		.189	
Modeled h' (cm) (Parameter Set 2)	.445	.385	.452	.388	.194	.129

Table 3. Measurements of the dome height h' for THUNDER actuators and model predictions with Parameter Set 1 (Manufacturer Specifications) and Parameter Set 2 (Estimated Parameters).

6. Concluding Remarks

This paper addresses the question (i) posed in the Introduction; namely, given a specified material composition and set of manufacturing conditions, what is the final shape of the THUNDER actuator? The primary mechanisms leading to the final curvature are the strains due to differing thermal properties of the component materials and the strains due to repoling. To quantify the thermal component, linear thermoelastic relations were assumed and force and moment balancing were employed to quantify the resulting curvature and in-plane strains. This accounts for approximately 85% of the final curvature of the actuator. The remaining changes in curvature are due to strains produced when dipole moments align with the applied electric field during repoling. This component is modeled through the application of domain theory for ferroelectric materials.

As indicated by the comparison with experimental data for THUNDER actuators, the combined model accurately quantifies both effects under a variety of conditions and hence provides the capability for predicting the final shape of the actuator. Hence it provides a useful tool for designing THUNDER actuators for various applications. We note that the accuracy of the model in some cases is dependent upon the estimation of the thermal coefficients and moduli of elasticity for the component materials. In cases where measured values for the saturation electrostriction are unavailable, this coefficient must also be estimated to quantify the effects of repoling. A comparison of model predictions with experimental results illustrates that once estimated, this coefficient is accurate for a variety of actuator configurations.

Acknowledgements

The research of H.T.B. and R.C.S. was supported in part by the Air Force Office of Scientific Research under the grant AFOSR-F49620-98-1-0180.

References

[1] B.A. Boley and J.H. Weiner, *Theory of Thermal Stresses,* John Wiley and sons, New York, 1960.

[2] D.L. Edberg, "Control of flexible structures by applied thermal gradients," *AIAA Journal*, 25(6), pp. 877-883, 1987.

[3] A. Hamamoto and M.W. Hyer, "Nonlinear temperature-curvature relationships for unsymmetric graphite epoxy laminates," *International Journal of Solids and Structures*, 23(7), pp. 919-935, 1987.

[4] M.W. Hyer, "The room-temperature shapes of four-layer unsymmetric cross-ply laminates," *Journal of Composite Materials*, 16(4), pp. 318-340, 1981.

[5] M.W. Hyer and A. Jilani, "Predicting the deformation characteristics of rectangular unsymmetrically laminated piezoelectric materials," *Smart Materials and Structures*, 7, pp. 1-8, 1998.

[6] B. Jaffe, W.R. Cook, Jr. and H. Jaffe, *Piezoelectric Ceramics*, Academic Press, New York, 1971.

[7] A.J. Moulson and J.M. Herbert, *Electroceramics*, Chapman and Hall, New York, 1990.

[8] S. Chikazumi, *Physics of Ferromagnetism*, Second Edition, Oxford University Press, New York, 1997.

[9] D.C. Jiles, *Introduction to Magnetism and Magnetic Materials*, Chapman and Hall, New York, 1991.

[10] R.G. Bryant, "LaRC^{TM}-SI: a soluble aromatic polyimide," *High Performance Polymers*, 8, pp. 607-615, 1996.

[11] K.M. Mossi, G.V. Selby and R.G. Bryant, "Thin-layer composite unimorph ferroelectric driver and sensor properties," *Materials Letters*, 35, pp. 39-49, 1998.